Dynamics of the Peel Front and the Nature of Acoustic Emission during Peeling of an Adhesive Tape

Rumi De[1] and G. Ananthakrishna[1,2]

[1]*Materials Research Centre, Indian Institute of Science, Bangalore 560012, India*
[2]*Centre for Condensed Matter Theory, Indian Institute of Science, Bangalore 560012, India*

(Received 9 December 2005; published 18 October 2006)

We investigate the peel front dynamics and acoustic emission (AE) of an adhesive tape within the context of a recent model by including an additional dissipative energy that mimics bursts of acoustic signals. We find that the nature of the peeling front can vary from a smooth to a stuck-peeled configuration depending on the values of dissipation coefficient, inertia of the roller, and mass of the tape. Interestingly, we find that the distribution of AE bursts shows power law statistics with two scaling regimes with increasing pull velocity as observed in experiments. In these regimes, the stuck-peeled configuration is similar to the ''edge of peeling'' reminiscent of a system driven to a critical state.

DOI: 10.1103/PhysRevLett.97.165503 PACS numbers: 62.20.Mk, 05.45.−a, 46.50.+a, 68.35.Np

The process of peeling of an adhesive material from a substrate is a complicated phenomenon involving molecular attraction at the interface and kinetic and dynamical effects. The kinetic nature of the process is clear from the fact that the peel force depends on the peel rate. The fracture process during peeling can be either cohesive or adhesive at low or high peel velocities, respectively. At intermediate velocities, the fracture process is intermittent, suggesting that the peeling process results from an interplay of time scales. At low peel velocities, there is sufficient time for viscoelastic glue to fully relax, while at high velocities, the glue essentially behaves like a solid [1]. The intermittent behavior is observed when the viscoelastic time scale is of the same order as the peel rate time scale. It is an everyday experience that the peeling process is always accompanied by a characteristic audible noise [2,3]. However, the mechanism leading to the acoustic emission (AE) has remained ill understood. Moreover, the inhomogeneous deformation of the peel front results from the destabilization of a uniformly advancing peel front [4]. To the best of our knowledge, we are not aware of any model that investigates the dynamics of the peeling front and the associated acoustic emission. We address these two issues within the context of a model for the peeling of an adhesive tape.

Experiments on peeling of an adhesive tape mounted on a roller [2] show that the peel force function has two stable branches separated by an unstable one. The pull force exhibits a rich variety of behavior ranging from sawtooth to irregular waveforms [2,5,6]. A dynamical analysis of the force waveforms and the AE signals reports chaotic dynamics at the upper end of pull velocities [7]. However, as there are no models, no further insight into the origin of acoustic emission has been possible.

A relevant model introduced in [2] has been subsequently studied by others (Refs. [3,5,6]); it belongs to the category of differential algebraic equations (DAE) and is singular, requiring an appropriate DAE algorithm provided in Ref. [8]. (For this reason, the results in Ref. [5] are the artifact of the method followed.) Recently, we modified these equations into a set of ordinary differential equations (ODE) by including the kinetic energy of the stretched tape. The ODE model not only supports dynamical jumps across the two stable branches, but also it displays a rich dynamics [9]. Here, we extend this model to include spatial degrees of freedom to study the contact line dynamics of the peeling front. The inclusion of a local strain rate dependent Rayleigh dissipation functional along with the kinetic energy of the tape forms a basis for converting the potential energy stored in the stretched tape into kinetic energy, providing a mechanism for explaining qualitative experimental features on AE [10,11].

Figure 1(a) shows a schematic representation of the experimental setup. An adhesive roller tape of radius R is mounted on an axis passing through O and is pulled at a constant speed V by a motor positioned at O'. Then, the line PQ represents the peeling front. Several features of the setup can be explained by considering the projection onto the plane of the paper (OPO'). The tangent to the contact point P (representing the contact line PQ) subtends an angle θ to the line PO'. Let the distance between O to O' be l and the peeled length of the tape PO' be L. If P subtends an angle α at O with the horizontal OO', the geometry of the setup gives $L\cos\theta = -l\sin\alpha$ and $L\sin\theta = l\cos\alpha - R$. As the local velocity v at P under-

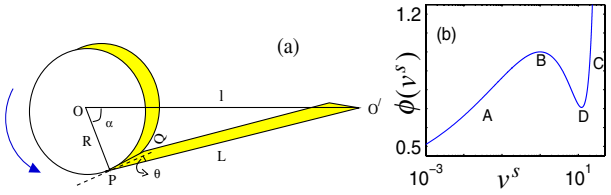

FIG. 1 (color online). (a) A schematic plot of the experimental setup. (b) Plots of $\phi(v^s)$ as a function of v^s for $V^s = 1.45$.

goes rapid bursts during rupture, we have $V = v + \dot{u} - \dot{L} = v + \dot{u} + R\cos\theta\dot{\alpha}$. Let $u(y)$ be the displacement with respect to the uniform "stuck" peel front, and let $v(y)$, $\theta(y)$, and $\alpha(y)$ be defined at every point y along the contact line. As the tape of width b is pulled with a velocity V, the above equation generalizes to

$$\frac{1}{b}\int_0^b [V - v(y) - \dot{u}(y) - R\cos\theta(y)\dot{\alpha}(y)]dy = 0. \quad (1)$$

However, as we are interested in the dynamics of the contact line of the softer glue material (whose elastic constant is 3 orders less than that of tape material), the effective spring constant k_g of the contact line is assumed to be much less than that of the tape material k_t. Then, as the entire tape is pulled with a velocity V, the force along PO' equilibrates fast, we can assume that the integrand in Eq. (1) is zero for all y.

We derive the equations of motion of the contact line by considering the Lagrangian $\mathcal{L} = U_K - U_P$, where U_K and U_P are the kinetic and potential energies, respectively. The kinetic energy is given by $U_K = \frac{1}{2}\int_0^b \xi[\dot{\alpha}(y) + \frac{v(y)}{R}]^2 dy + \frac{1}{2}\int_0^b \rho[\dot{u}(y)]^2 dy$, where the first term represents the rotational kinetic energy of the roller tape and second term arises due to the kinetic energy of the stretched part of the tape. Here, ξ is the moment of inertia per unit width of the roller tape and ρ the mass per unit width of the length L. The total potential energy (PE) U_P of the stretched ribbon can be written as $U_P = \frac{1}{2}\int_0^b \frac{k_t}{b}[u(y)]^2 dy + \frac{1}{2}\times \int_0^b k_g b[\frac{\partial u(y)}{\partial y}]^2 dy$. The total dissipation has two contributions, $\mathcal{R}_{\rm AE} = \frac{1}{b}\int_0^b \int f(v(y))dv dy + \frac{1}{2}\int_0^b \frac{\Gamma_u}{b}[\frac{\partial \dot{u}(y)}{\partial y}]^2 dy$, where $f(v)$ physically represents the peel force function assumed to be derivable from a potential function $\Phi(v) = \int f(v)dv$ (see Ref. [9]). The second term, denoted by $\mathcal{R}_{\rm AE}$, represents the dissipation arising from the rapid movement of peel front given by the Rayleigh dissipative functional. This has the same form as the energy dissipated in the form of acoustic emission during abrupt motion of dislocations in plastic deformation, i.e., $E_{\rm AE} \propto \dot{\epsilon}^2(r)$, where $\dot{\epsilon}(r)$ is the local plastic strain rate [10]. Hence we interpret $\mathcal{R}_{\rm AE}$ as the energy dissipated in the form of AE signals. Indeed, such a term has been successfully used to explain several features of AE signals in martensites [11].

We rewrite all the energy terms in a scaled form using a timelike variable $\tau = \omega_u t$, where $\omega_u^2 = k_t/(b\rho)$. Let $f_{\rm max}$ and $v_{\rm max}$ be the maximum value of $f(v)$ and v on the left stable branch. Then, defining a length scale $d = f_{\rm max}/k_t$, we introduce $u = Xd = X(f_{\rm max}/k_t)$, $l = l^s d$, $L = L^s d$, and $R = R^s d$. The peel force f can be written as $f = f_{\rm max}\phi(v^s)$, where $v^s = v/v_c\omega_u d$ and $V^s = V/v_c\omega_u d$ are the dimensionless peel and pull velocities, respectively. Here, $v_c = v_{\rm max}/\omega_u d$ is the dimensionless critical velocity at which the unstable branch starts (in the scaled units, the unstable branch begins at $v^s = 1$). Defining $C_f = (f_{\rm max}/k_t)^2(\rho/\xi)$, $k_0 = k_g b^2/(k_t a^2)$, $\gamma_u = \Gamma_u\omega_u/(k_t a^2)$, and $y = ar$, where a is a unit length variable along the peel front, the scaled local form of Eq. (1) is

$$\dot{X} = (V^s - v^s)v_c + R^s\frac{l^s}{L^s}(\sin\alpha)\dot{\alpha}. \quad (2)$$

The scaled kinetic and potential energies can be written as $U_K^s = \frac{1}{2C_f}\int_0^{b/a}[\dot{\alpha}(r) + \frac{v_c v^s(r)}{R^s}]^2 dr + \frac{1}{2}\int_0^{b/a}[\dot{X}(r)]^2 dr$ and $U_P^s = \frac{1}{2}\int_0^{b/a} X^2(r)dr + \frac{k_0}{2}\int_0^{b/a}[\frac{\partial X(r)}{\partial r}]^2 dr$, respectively. The total dissipation in a scaled form is $\mathcal{R}^s = \frac{1}{b}\times \int_0^{b/a}\int \phi(v^s(r))dv^s dr + \frac{1}{2}\int_0^{b/a}\gamma_u[\frac{\partial \dot{X}(r)}{\partial r}]^2 dr$. $\phi(v^s)$ is the scaled peel force that can be obtained by using in Eq. (9) of Ref. [9] shown in Fig. 1(b). We shall refer the left branch AB as the "stuck state" and the high velocity branch CD as the peeled state.

Using $\alpha(r)$, $\dot{\alpha}(r)$, $X(r)$, and $\dot{X}(r)$ as generalized coordinates in the Lagrange equations of motion, $\frac{d}{d\tau}\times(\frac{\partial \mathcal{L}}{\partial \dot{\alpha}(r)}) - \frac{\partial \mathcal{L}}{\partial \alpha(r)} + \frac{\partial \mathcal{R}^s}{\partial \dot{\alpha}(r)} = 0$ and $\frac{d}{d\tau}(\frac{\partial \mathcal{L}}{\partial \dot{X}(r)}) - \frac{\partial \mathcal{L}}{\partial X(r)} + \frac{\partial \mathcal{R}^s}{\partial \dot{X}(r)} = 0$, we get the equations of motion as

$$\ddot{\alpha} = -\frac{v_c\dot{v}^s}{R^s} - C_f R^s\frac{l^s/L^s\sin\alpha}{(1 + l^s/L^s\sin\alpha)}\phi(v^s), \quad (3)$$

$$\ddot{X} = -X + k_0\frac{\partial^2 X}{\partial r^2} + \frac{\phi(v^s)}{(1 + l^s/L^s\sin\alpha)} + \gamma_u\frac{\partial^2 \dot{X}}{\partial r^2}. \quad (4)$$

Equations (3) and (4) are still not suitable for further analysis as they have to satisfy the constraint equation (2). In the spirit of mechanical systems with constraints [12], we obtain the equation for the acceleration variable $\dot{v}^s(r)$ by differentiating Eq. (2) to be

$$\dot{v}^s = \frac{(-\ddot{X} + \frac{R^s l^s}{L^s}\{\dot{\alpha}^2[\cos\alpha - R^s l^s(\frac{\sin\alpha}{L^s})^2] + \sin\alpha\ddot{\alpha}\})}{v_c}. \quad (5)$$

Equations (2), (3), and (5) were solved by discretizing and using an adaptive step size stiff differential equations solver (MATLAB package) for open boundary conditions. The initial conditions were chosen from the stuck state [i.e., AB branch of $\phi(v^s)$] with a small spatial inhomogeneity in X that approximately satisfies Eq. (2). The system is evolved until a steady state is reached before the data are accumulated. We have studied the dynamics over a wide range of values of C_f, V^s, and γ_u keeping $R^s = 0.35$, $l^s = 3.5$, $k_0 = 0.1$, $N = 50$, and $N = 100$. Note that v_c is an important parameter which, however, is determined once $f(v)$ is given. [The values of the unscaled parameters, for example, $k_t \sim 1000$, are fixed using the data in Ref. [13]. $f(v)$ used here preserves the major features of the experimental curve such as $f_{\rm max} \sim 280$ N/m at $v_{\rm max} = 0.05$ cm/s with a velocity jump to 16 cm/s. See also [8]. Note, however, we do not use the dynamization scheme used in [8].] These equations exhibit rich dynamics which can be classified as the uniform, rugged, and stuck-peeled nature of the contact line. In the unscaled variables, the results reported here correspond to changing the tape mass ($m = \rho b$) while keeping $I(= \xi b)$ constant.

First, consider the results for $C_f = 0.007\,88$ ($v_c = 0.0024$) and $V^s = 1.45$ (i.e., high inertia, low mass, and

low pull velocity regime in the unscaled parameter space) as we decrease the dissipation parameter γ_u from 1.0 to 0.001. We observe a wide variety of events, some of which are illustrated in the plots of the peel velocities $v_i^s(\tau)$. For instance, all spatial points peel together for $\gamma_u = 1.0$. As we decrease γ_u to 0.1, keeping other parameters fixed, the contact line profile becomes rugged even though all points peel nearly at the same time as seen in Fig. 2(a).

Intuitively, high γ_u implies that velocities of neighboring points are coupled strongly and hence are not allowed to follow their local site dynamics. Thus, the total dissipation $\mathcal{R}^s_{\rm AE}(\tau) = \frac{1}{2}\gamma_u \sum_i (\dot{X}_{i+1} - \dot{X}_i)^2$ is vanishingly small when peeling is coherent. In contrast, for low γ_u [say, 0.1 as in Fig. 2(a)], the coupling between neighboring velocities is weak and the local dynamics dominates. This means more ruggedness and hence higher dissipation.

As γ_u is decreased to 0.01, the peel front exhibits two types of configurations depending on whether the system is on the *AB* branch entirely, or partly on both the *CD* and *AB* branches of ϕ. When on the *CD* branch, the ruggedness is substantially higher than that for $\gamma_u = 0.1$ [Fig. 2(a)]. Once the peeling process starts, the peel front breaks up into regions of stuck and peeled segments as shown in Fig. 2(b). This configuration results from the orbit jumping between the low and high velocity branches of $\phi(v^s)$. A typical phase plot of X_i^s versus v_i^s is shown in Fig. 3(a) for $i = 25$ with other points differing only in phase. Thus, as the phase difference along the peel front builds up to a value equal to the phase difference between the orbits that are in the stuck and the peeled states, the stuck state changes to a peeled state or vice versa.

Now consider the dynamics for higher mass ($C_f = 0.788$, $v_c = 0.024$) and $V^s = 1.45$ as we decrease $\gamma_u = 1.0$ to 0.001. For this entire range of γ_u, the peel front displays stuck-peeled segments for all times as shown in Fig. 3(b). There is a dynamic equilibrium between the peeled and stuck segments with the segments that are stuck at some instant getting unstuck at another instant and vice versa. Further, as is clear from Fig. 3(b), the average of the velocity jumps along the peel front is smaller than the low mass case (compare Fig. 2). Concomitantly, the number of stuck segments increases with each stuck segment having a only few stuck points better illustrated in an instantaneous plot of $v_i^s - 1$ shown in Fig. 3(c). Moreover, from Fig. 3(c), it is clear that even the points that are in the stuck state are barely stuck. Further, it is clear that the orbit spends considerable time around the maximum which is the critical peel value [Fig. 3(d)]. Thus, Figs. 3(b) and 3(c) correspond to the verge of a peeling state. The "edge of peeling" picture remains unaltered with time even though the stuck points themselves change. The largest Lyapunov exponent is 0.15 (for $N = 50$) and hence this state is spatiotemporally chaotic [Fig. 4(a)].

In experiments, the nature of the AE signals changes from burst type to continuous type as the pull velocity is increased. In the model, the rate of dissipated energy $\mathcal{R}^s_{\rm AE} = -dE_{\rm AE}/d\tau$ represents the AE bursts. We have studied the statistics of $\mathcal{R}^s_{\rm AE}$ as we increase the pull velocity keeping the tape mass low ($C_f = 0.007\,88$, $v_c = 0.0024$). As in experiments, for small γ_u, at low velocities, we find that $\mathcal{R}^s_{\rm AE}$ exhibits bursts followed by a quiescent state as shown in Fig. 4(b), which is similar to Fig. 4(a) of Ref. [3] (for the AE amplitudes). [$\mathcal{R}^s_{\rm AE}$ shown in Fig. 4(b) corresponds to Fig. 2(b).] In contrast, for high pull velocities and low mass, and for a range of γ_u, $\mathcal{R}^s_{\rm AE}$ exhibits continuous bursts as shown in Fig. 4(c), which is again seen in experiments [Fig. 4(b) of Ref. [3]]. High mass and low pull velocity also exhibits continuous bursts.

Denoting E_R to be the amplitude of $\mathcal{R}^s_{\rm AE}$ (i.e., from a maximum to the next minimum), for high pull velocities and low tape mass ($C_f = 0.0078$, $v_c = 0.0024$, $V^s = 5.93$), we find that the distribution of the magnitudes $D(E_R)$ shows a power law for all values of γ_u investigated, i.e., $D(E_R) \sim E_R^{-m_E}$. Further, $D(E_R)$ shown in Fig. 4(d) exhibits two distinct scaling regimes as for case of the distribution of the AE amplitudes (A) in experiments. The value of $m_E \sim 0.6$ for the small amplitude regime,

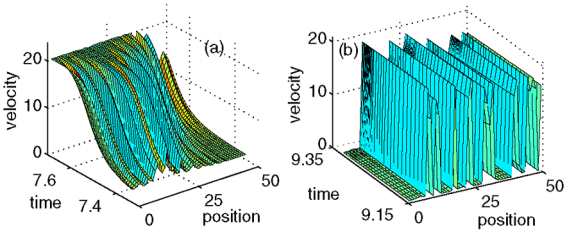

FIG. 2 (color online). Plot of the peel velocity configuration for $C_f = 0.007\,88$ and $V^s = 1.45$. (a) A rugged peel front for $\gamma_u = 0.1$. (b) Illustration of a stuck-peeled configuration for $\gamma_u = 0.01$.

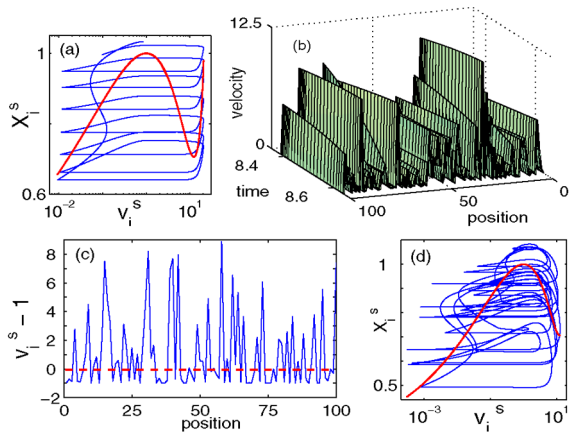

FIG. 3 (color online). (a) The phase plot for $i = 25$ for $C_f = 0.007\,88$ and $V^s = 1.45$, and $\gamma_u = 0.01$. (b) Plot of an "edge of peeling" configuration for $C_f = 0.788$, $V^s = 1.45$, and $\gamma_u = 0.01$. (c) The corresponding instantaneous plot of an edge of peeling configuration. The dashed line represents the critical peel velocity $v^s_{\rm max} = 1$. (d) The corresponding phase plot for $i = 25$. The bold lines in (a) and (d) represent $\phi(v_i^s)$.

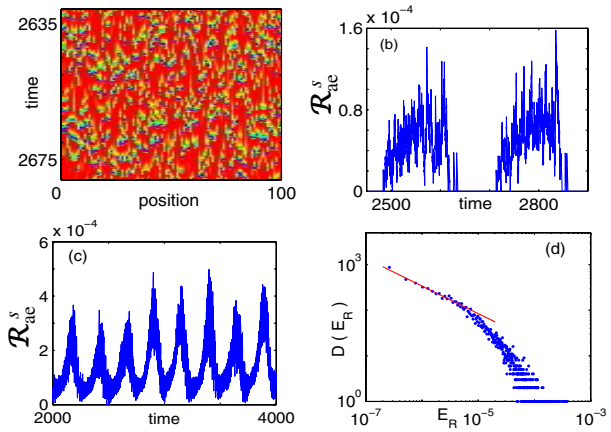

FIG. 4 (color online). (a) Spatiotemporal chaotic plot for $C_f = 0.788$, $V^s = 1.45$, and $\gamma_u = 0.01$ (low → high peel velocity: red → yellow → green → blue → pink; in gray levels, dark to white corresponds to low to high peel velocity). (b) Plots of $\mathcal{R}^s_{\mathrm{AE}}(\tau)$ vs time τ for $C_f = 0.007\,88$, $V^s = 1.45$, and $\gamma_u = 0.01$. (c) $\mathcal{R}^s_{\mathrm{AE}}(\tau)$ for $C_f = 0.007\,88$, $V^s = 5.93$, and $\gamma_u = 0.01$. (d) The corresponding distribution $D(E_R)$ of the amplitudes E_R showing two scaling regimes.

while that for large amplitudes that has a substantial scatter is about 1.8. The corresponding exponent values are $m_A \sim 0.3$ and 3.2 [13]. Using the fact that energy $E \propto A^2$, we get $m_E = (1 + m_A)/2$. Inserting the values of m_A, we get the corresponding exponents to be $m_E \sim 0.65$ and $m_E \sim 2.1$, which are close to the values predicted by the model considering the scatter for the latter. In contrast, for the high mass and low velocity case, we find a single scaling regime with an exponent $m_E \sim 0.69$.

Thus, several qualitative features of the peel front dynamics observed in experiments are reproduced by the model. For example, the characteristic features of the AE signals observed in experiments; namely, noisy AE bursts for low pull velocity changing over to continuous bursts at high pull velocity are reproduced. For high pull velocities (low tape mass), $D(E_R)$ exhibits two scaling regimes. However, comparison with experiments is made difficult due to the paucity of quantitative results except for the values of the exponents in the two scaling regimes, which is in reasonable agreement with the model. Even so, our study suggest that if one wants a smooth peeling, one should peel at low velocity using high viscous dissipation. Significantly, the power law is seen at high pull speeds and thus is unlike self-organized criticality.

The power law statistics for high pull velocities arises as a competition among the time scales due to the inertia of the tape, dissipation, and imposed velocity, which is small at high V^s, leaving very little time for internal degrees of freedom to relax. The nature of the peel front ranges from synchronous peeling for large γ_u to the rugged type for small γ_u. The "stuck-peeled" configuration is qualitatively similar to the inhomogeneous peel fronts observed in experiments [4] as also to the thin viscous film interface [14]. Interestingly, the "verge of peeling picture" of the peel front [Figs. 3(b) and 3(c)] is similar to the edge of unpinning picture of dislocations in the Portevin–Le Chatelier effect [15]. This is one of the few cases where the power law emerges purely from deterministic dynamics.

Here, it is worth commenting on the assumption that the integrand of Eq. (1) vanish at each point y which is valid when $L \gg b$ and when shear modulus k_G is small. In principle, one should have a long range term of the form $k_G \int_0^b [u(y) - u(y')]^2 dy dy'/2|y - y'|$. An equilibrium calculation with $u(y)$ defined at one end shows that the shear strain energy is less than 1% compared to the total even for not too small $b/L = 0.2$. This lends support for the PE term used. We have also carried out numerical calculations by retaining this term. For small k_G, results are not affected as it should be expected. However, for relatively high values of k_G, the solutions that were smooth break up into stuck-peeled configurations.

Here, the adhesive properties of the glue are included only in an indirect way through the peel force function (and low effective spring constant of the peel front due to adhesive glue) and that of AE through the Rayleigh dissipation function. While the model recovers most dynamical features of peeling, issues that depend critically on the finite thickness of the adhesive material (fibril formation) cannot be addressed within the scope of the model.

We thank Professor A. J. Beaudoin for helpful discussions. G. A. acknowledges BRNS Grant No. 2005/37/16/BRNS.

[1] P. G. de Gennes, Langmuir **12**, 4497 (1996).
[2] D. Maugis and M. Barquins, in *Adhesion 12*, edited by K. W. Allen (Elsevier, London, 1988), p. 205.
[3] M. Ciccotti *et al.*, Int. J. Adhes. Adhes. **24**, 143 (2004).
[4] C. Gay and L. Leibler, Phys. Today **52**, No. 11, 48 (1999); Phys. Rev. Lett. **82**, 936 (1999).
[5] D. C. Hong and S. Yue, Phys. Rev. Lett. **74**, 254 (1995).
[6] M. Ciccotti, B. Giorgini, and M. Barquins, Int. J. Adhes. Adhes. **18**, 35 (1998).
[7] M. C. Gandur, M. U. Kleinke, and F. Galembeck, J. Adhes. Sci. Technol. **11**, 11 (1997).
[8] Rumi De, Anil Maybhate, and G. Ananthakrishna, Phys. Rev. E **70**, 046223 (2004).
[9] Rumi De and G. Ananthakrishna, Phys. Rev. E **71**, 055201(R) (2005).
[10] Rumi De and G. Ananthakrishna, Europhys. Lett. **66**, 715 (2004).
[11] R. Ahluwalia and G. Ananthakrishna, Phys. Rev. Lett. **86**, 4076 (2001); S. Sreekala and G. Ananthakrishna, *ibid.* **90**, 135501 (2003).
[12] E. C. G. Sudarshan and N. Mukunda, *Classical Dynamics: A Modern Perspective* (John Wiley and Sons, New York, 1974).
[13] M. Ciccotti (private communication).
[14] A. Ghatak *et al.*, Phys. Rev. Lett. **85**, 4329 (2000).
[15] G. Ananthakrishna and M. S. Bharathi, Phys. Rev. E **70**, 026111 (2004).